

Simulating Floquet topological phases in static systems

S. Franca^{1*}, F. Hassler², I. C. Fulga¹

¹ IFW Dresden and Würzburg-Dresden Cluster of Excellence ct.qmat, Helmholtzstr. 20,
01069 Dresden, Germany

² JARA-Institute for Quantum Information, RWTH Aachen University, 52056 Aachen,
Germany

* s.franca@ifw-dresden.de

March 25, 2022

Abstract

We show that scattering from the boundary of static, higher-order topological insulators (HOTIs) can be used to simulate the behavior of (time-periodic) Floquet topological insulators. We consider D -dimensional HOTIs with gapless corner states which are weakly probed by external waves in a scattering setup. We find that the unitary reflection matrix describing back-scattering from the boundary of the HOTI is topologically equivalent to a $(D-1)$ -dimensional nontrivial Floquet operator. To characterize the topology of the reflection matrix, we introduce the concept of ‘nested’ scattering matrices. Our results provide a route to engineer topological Floquet systems in the lab without the need for external driving. As benefit, the topological system does not suffer from decoherence and heating.

Contents

1	Introduction	2
2	Main idea	3
3	Hamiltonian and scattering matrix	4
4	Nested scattering matrices and topological invariants	7
5	Disorder effects	8
6	Experimental feasibility	9
7	Conclusion	10
A	Calculating the reflection matrix	11
B	Symmetries of the reflection matrix	11
C	Topological phase transitions of the reflection matrix	13

1 Introduction

Topology provides a common tool set for analyzing the properties of both static and dynamical systems. Bulk-boundary correspondence predicts the appearance of gapless modes both in the spectra of time-independent Hermitian Hamiltonians [1, 2], as well as in those of the unitary time-evolution (or Floquet) operators describing periodically-driven systems [3, 4]. Both Hermitian and unitary phases have been classified using dimensional reduction, leading to the so called ‘periodic tables’ of topological phases [5–15].

In spite of the common methods used in their analysis, there is a strong dichotomy between the study of topology in Hermitian and unitary systems, both on a theoretical and especially on an experimental level. Topological phases described by Hamiltonians are usually realized in the ground states of isolated, time-independent systems [1, 2], and a large body of research has focused on materials that exhibit topological nontrivial ground states [16–22]. In contrast, unitary topology conventionally refers to Floquet operators that physically involve pumping energy into an open system by means of an external driving field. In the many-body setting, it is known that the system will absorb this energy, reaching a featureless steady state unless it is many-body localized [23, 24]. Even on the single-particle level, heating due to noise-induced decoherence of Floquet states is unavoidable, since any realistic driving field will not be perfectly periodic in time [25–27].

In this work, we resolve the dichotomy between Hermitian and unitary systems by showing that a static, D -dimensional topological phase can be used to simulate a time-periodic, $(D-1)$ -dimensional topological phase, without any external driving. We consider a sub-class of higher-order topological insulators (HOTIs) [28–34]: time-independent systems with a gapped bulk, gapped boundaries, and topologically protected gapless modes localized at their corners. We envision a scattering experiment on the D -dimensional HOTI by probing the system at the boundary. Due to the gap, all incoming modes are back-reflected, a process described by a reflection matrix r (see Fig. 1). Our main insight is that this reflection matrix: (1) is unitary, (2) $(D-1)$ -dimensional, (3) has a gapped spectrum, and (4) shows topologically protected mid-gap modes at its boundaries. As such, the unitary reflection matrix can be thought of as the Floquet operator of a lower-dimensional driven system.

On a practical level, our results provide a way of experimentally realizing unitary topological phases in a static experiment. The required ingredients, a HOTI probed by means of a scattering measurement, are presently available in the lab. HOTIs have been achieved in a variety of metamaterials [35–50]. The reflection matrix can be determined by standard interferometric techniques [51, 52], or by simply visualizing the standing wave pattern formed between incoming and outgoing modes [49, 53]. Note that alternative proposals for simulating Floquet phases, such as photonic crystals [54–57] or quantum walks [58, 59], suffer from decoherence due to noise in the periodic modulation of the system. In contrast, our setup has the advantage of avoiding decoherence. This is because there is no driving field to begin with: the HOTI is fully static and remains in its ground state, being only weakly probed.

We first present our main idea in a generic setting (Sec. 2) before proceeding with a

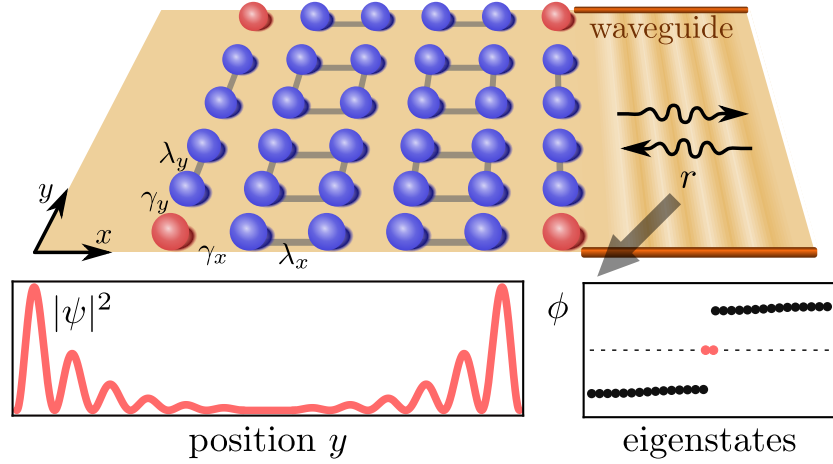


Figure 1: Scattering experiment in which a waveguide is attached to the right boundary of a HOTI [Eq. (1)] with corner states (red). Due to the gapped bulk and edges, the incoming waves are reflected. This process is described by the unitary reflection matrix r , that is topologically equivalent to the Floquet operator of a nontrivial 1D chain. The spectrum of its eigenphases ϕ , denoting the phase difference between incoming and reflected waves, exhibits topologically protected mid-gap states. The corresponding transversal modes ψ are localized at the boundaries of the waveguide and scatter off the corners of the 2D system.

concrete example of a two-dimensional (2D) particle-hole symmetric HOTI. For the latter system, we show that the reflection matrix is topologically equivalent to a 1D Floquet Kitaev chain [60–62], realizing the same topological phases (Sec. 3). By interpreting the reflection matrix as a 1D Floquet operator and computing its scattering matrix (e.g., the scattering matrix of the reflection matrix) [63, 64], we determine the topological invariants (Sec. 4). This defines a generic, recursive procedure similar to that of ‘nested Wilson loops’ [28, 29]. It enables to access the unitary topology encoded in a scattering matrix by computing its higher-order, nested scattering matrices. We show that the resulting topological phases are robust against disorder as long as their protecting symmetries are preserved (Sec. 5). We argue that the topological phases can be identified using experimental tools which have already been demonstrated (Sec. 6). We conclude and discuss future directions of research in Sec. 7. The appendix is dedicated to details on how we compute the scattering matrix (App. A), its symmetries (App. B), and its topological phase transitions (App. C).

2 Main idea

Consider the 2D HOTI shown in Fig. 1, which has gapped bulk and edges, shown in blue, but hosts topologically protected gapless corner modes, shown in red. The right edge of this static system, having a linear dimension of L sites, is weakly coupled to a waveguide with a set of L modes that are used to probe the system. Since the bulk and the edges of the HOTI are fully gapped, no transmission occurs through the system, and all incoming waves are back-reflected. Therefore, the reflection matrix r , whose elements $(r)_{nm}$ describe the probability amplitude to scatter from (incoming) mode m to (outgoing) mode n , is forced to

be unitary. The eigenvalues $e^{i\phi}$ of this matrix determine the eigenphases ϕ acquired by modes upon reflecting from the system edge.

Consider an incoming plane-wave, extended along the translationally invariant direction of the waveguide, but localized in its transversal direction y (see Fig. 1). The phase it acquires upon reflection will depend on the transversal direction. If the reflection occurs from a portion close to the middle of the gapped edge, we expect the outgoing state to pick up an eigenphase ϕ , which may depend on the properties of the edge close to the position y and its coupling to the waveguide. In fact, for the choice of system and waveguide considered in the following, we have an open boundary condition with $\phi \rightarrow 0$ for vanishingly weak coupling strength. In contrast, if the incoming plane-wave is localized at the boundary of the waveguide, such that it impinges on the corner of the HOTI, then resonant scattering from the gapless corner mode will force the outgoing state to pick up a π -phase relative to the incoming one [65–68]. As a result, the eigenstates of r at the center of the waveguide have eigenphases ϕ close to zero, and there is one eigenvalue with $\phi = \pi$ located at each of the two boundaries of the waveguide. The reflection matrix of this 2D system thus corresponds to a 1D topological Floquet chain (along the transversal direction) with mid-gap topological modes (at $\phi = \pi$) localized at the ends of the chain. Note that the π -modes are specific to the classification of unitary Floquet systems and do not have an analog for Hamiltonian systems. Thus, the process of weakly probing a static HOTI is determined by the reflection matrix r , which is equivalent to a Floquet operator. If the static system is in the HOTI phase, the resulting Floquet operator is also topological; this is the sense in which the static system simulates a topological Floquet system.

By analogy, we expect the connection between the topology of the Hamiltonian and that of the reflection matrix to remain valid in arbitrary dimension: a d -dimensional HOTI in which the bulk and hypersurfaces are gapped, but which hosts gapless 0D corner modes at its 2^d corners, will have a reflection matrix that simulates a $(d-1)$ -dimensional topological Floquet system. As in the 2D example of Fig. 1, this is because waves which are back-scattered from the corners will produce π -modes in the reflection matrix, whereas waves reflected from the middle of the surface of the system will produce modes with $\phi \rightarrow 0$ in the weak-coupling limit.

3 Hamiltonian and scattering matrix

To make the above discussion concrete, we consider a HOTI model describing non-interacting, spinless fermions hopping on a dimerized square lattice [28, 29]. There are four sites per unit cell, and each plaquette is threaded by a magnetic π -flux. The Hamiltonian reads

$$h(\mathbf{k}) = (\gamma_x + \lambda_x \cos k_x) \tau_x \sigma_0 - \lambda_x \sin k_x \tau_y \sigma_z - (\gamma_y + \lambda_y \cos k_y) \tau_y \sigma_y - \lambda_y \sin k_y \tau_x \sigma_x, \quad (1)$$

where $\mathbf{k} = (k_x, k_y)$ are the momenta in the two directions. The Pauli matrices τ act on the sublattice degree of freedom, whereas the Pauli matrices σ act on the two sites within a sublattice. Similar to the Su-Schrieffer-Heeger (SSH) model [69], the hoppings in the horizontal and vertical (x and y) directions are dimerized, taking values $\gamma_{x,y}$ within a unit cell and $\lambda_{x,y}$ between unit cells, all chosen real and positive in the following. The model obeys particle-hole symmetry, $\mathcal{P} = \tau_z \mathcal{K}$, with \mathcal{K} complex conjugation, such that all states are symmetric in energy around $E = 0$.¹ For $\gamma_{x,y} < \lambda_{x,y}$ the system is in a topological phase: the bulk/edges

¹Note that the system has an additional chiral symmetry, $\mathcal{C} = \tau_z$, which has no effect as we do not consider more than a single 0- or π -mode. For more information see Appendix B.

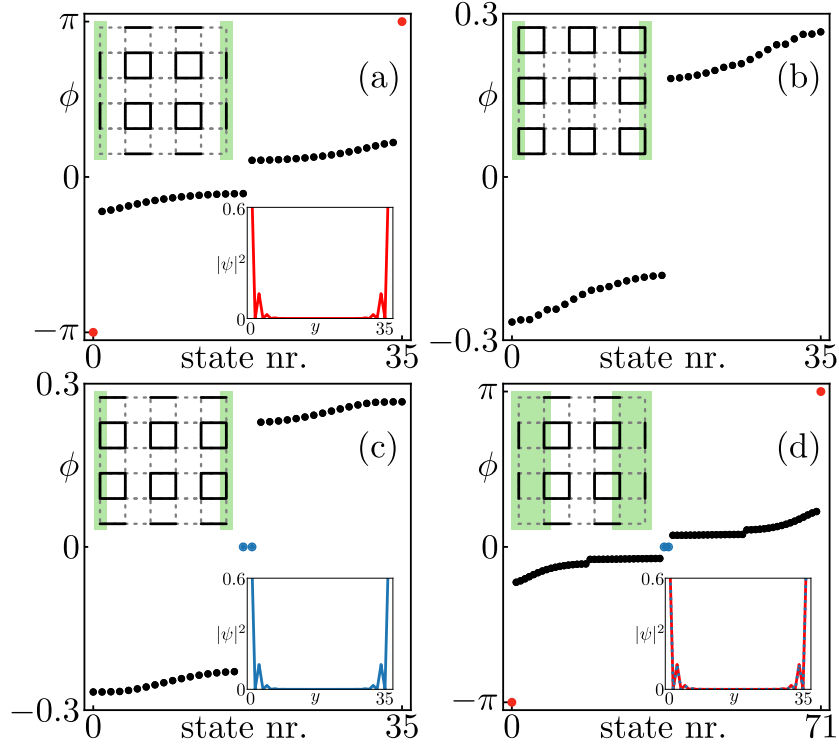


Figure 2: Eigenphases of the reflection matrix, showing π -modes (0-modes) and their associated wavefunctions in red (blue). The HOTI parameters are $\lambda_{x,y} = 1$ in all panels. We have chosen $\gamma_{x,y} = 0.4$ in panels (a) and (d), $\gamma_{x,y} = 1.2$ in panel (b), whereas $\gamma_x = 1.2$ and $\gamma_y = 0.4$ in panel (c). Insets sketch the corresponding dimerization pattern of the HOTI as well as the sites connected to the lead (green). The system-lead coupling strength is $t_{sl} = 0.5$ in all cases. The gap around $\phi = 0$ as well as the bandwidth of the bulk states (black) is proportional to t_{sl} in the weak coupling limit.

are gapped and corner sites are weakly coupled to the rest of the system (see Fig. 1) such that they each host a localized, zero-energy mode.

We place a finite-sized HOTI ($L \times L$ sites with $L = 36$) in a two-terminal geometry with translationally invariant electronic waveguides (leads) oriented in the x direction attached to its left- and right-most sites. Incoming and outgoing modes at $E = 0$ are related by the scattering matrix,

$$S = \begin{pmatrix} r & t' \\ t & r' \end{pmatrix}, \quad (2)$$

where the blocks $r^{(l)}$ and $t^{(l)}$ contain the probability amplitudes for states to be back-reflected or transmitted across the system, respectively. More details on calculating S can be found in Appendix A. To obtain direct information on the real-space position of a scattering state in the y direction, we choose a simple model for the leads composed of decoupled chains (zero on-site term, unit hopping), each chain connecting to a single site of the edge of the system. As a result, the reflection and transmission blocks have a size $L \times L$ and are effectively 1D operators parameterized by the transversal coordinate y .

In the nontrivial phase, transmission through the system is exponentially suppressed since the bulk and edges are gapped. Hence, the reflection matrix r of the left lead (or equivalently

r' for the right lead) is unitary up to exponential precision. By numerically² diagonalizing the 1D unitary operator r , we find that its eigenphase spectrum is analogous to the eigenphase (or quasi-energy) spectrum of 1D Floquet topological chains, as shown in Fig. 2a. We observe two $\pm\phi$ -symmetric phase-bands, shown in black, separated by phase-gaps centered around $\phi = 0$ and $\phi = \pi$. The bands correspond to states which are back-reflected from the mid section, or ‘bulk’ of the lead, meaning states which contact the central part of the HOTI edge. At $\phi = \pm\pi$, however, there are two degenerate states, shown in red, which are separated by a gap from other eigenphases. These two modes correspond to scattering states at the boundaries of the lead and contact the corner states of the HOTI.

The reflection matrix r is topologically equivalent to a 1D nontrivial Floquet system and thus provides an example of dimensional reduction from a 2D Hermitian operator to a 1D unitary operator. The latter is in a symmetry class allowing for nontrivial topology, since it inherits particle-hole symmetry from the original 2D HOTI. The \mathcal{P} symmetry of the Hamiltonian and of the leads implies a constraint on the reflection matrix, $r = \tau_z r^* \tau_z$ [67, 71], which is identical to the condition imposed by particle-hole symmetry on Floquet systems [3, 63]. Due to the constraint relating r to its complex conjugate, the eigenvalues of r must be either real, corresponding to phases $\phi = 0, \pi$, or must come in complex conjugate pairs. This explains both the $\pm\phi$ -symmetric spectrum of Fig. 2 and the pinning of edge modes to the middle of the gap. Furthermore, since resonant scattering from a zero-energy state produces a π phase shift of the reflected wave [67], the corner states of a nontrivial HOTI induce topological π -modes in the reflection operator. Therefore, the dimensional reduction scheme obeys the requirement of mapping a nontrivial system onto a nontrivial one.

Particle-hole symmetric Floquet systems in 1D possess a $\mathbb{Z}_2 \times \mathbb{Z}_2$ classification [72], with four possible phases: (1) trivial, (2) edge modes at $\phi = \pi$, (3) edge modes at $\phi = 0$, and (4) a so-called ‘anomalous’ phase hosting edge modes at both 0 and π . Depending on the dimerization pattern of the 2D system and on how the leads are attached, we show that all four phases can be reproduced by the reflection matrix. As an immediate check, a trivial system, $\gamma_{x,y} > \lambda_{x,y}$, yields a trivial r (Fig. 2b). The phase with $\phi = 0$ modes (Fig. 2c) can be obtained by setting $\gamma_x > \lambda_x$ and $\gamma_y < \lambda_y$ (nontrivial dimerization on the edge contacting the leads, but trivial dimerization along the other edges). In this situation, the system is in a topological phase (as signaled by its nontrivial nested Wilson loop invariant [28]) even though it does not exhibit zero-energy corner states. Remarkably, the reflection matrix detects the topology of the phase in even in this case, by the presence of the $\phi = 0$ modes.

So far, the waveguides were only coupled to the outermost sites of the HOTI. Thus, only half of the sites of the last unit cell are coupled to the lead, since the unit cell contains four sites and only two of them form the boundary of the system (see Fig. 1). However, depending on the physical system realizing the HOTI phase, the matrix structure of the Hamiltonian Eq. (1) might be due to internal degrees of freedom. For instance, the Pauli matrices τ and σ could represent, e.g., electron-hole and spin degrees of freedom in a superconductor. In this case, a lead would couple to all four states in a unit cell, producing a reflection matrix which is $2L \times 2L$. Interestingly, attaching the lead in this way maps the nontrivial HOTI ($\gamma_{x,y} < \lambda_{x,y}$) to an anomalous r , with mid-gap end modes at both $\phi = 0$ and $\phi = \pi$ (Fig. 2d). Even though the system Hamiltonian is in the same nontrivial phase as was used to produce Fig. 2a, r is now in a different topological phase. The difference is due to the fact that,

²We use the kwant code for tight-binding and scattering matrix calculations [70]. The code used to generate our numerical results is included in the supplemental material.

both for static and for Floquet chiral systems [28, 29, 69, 73–77], the topology is not just a property of the HOTI Hamiltonian, but crucially depends on the way in which the system is terminated. The important point however, as discussed before, is that zero-energy corner states in the 2D HOTI lead to π modes in the reflection matrix, such that a nontrivial static system is mapped onto a nontrivial unitary Floquet operator.

4 Nested scattering matrices and topological invariants

We want to prove that the reflection matrix r of the HOTI is indeed in a topological phase when viewed as a unitary Floquet operator by computing its topological invariants. The spectra shown in Fig. 2 give a first indication that this is the case, due to the presence of mid-gap modes. We cannot employ the most conventional way of calculating the invariants of a periodically-driven system [9, 78], as we do not have access to the instantaneous eigenstates of the system at every moment of time throughout a period of the drive. In contrast, in our system we only access the reflection matrix r , which is analogous to the Floquet operator — the time-evolution operator over a full driving cycle. Recently, a way of determining the topological invariants of a 1D Floquet system has been devised [63, 64] which only relies on knowledge of r (the analog of the Floquet operator). To this end, we calculate the scattering matrix \tilde{S} of a 1D Floquet system described by the ‘Floquet operator’ r . We call \tilde{S} a nested scattering matrix, as it is the scattering matrix of the reflection matrix r (which is a sub-block of the scattering matrix S).

Following Ref. [63], the procedure to obtain the topological invariants is as follows: we define a fictitious scattering problem starting from the finite-sized, 1D unitary operator r . We attach one fictitious absorbing terminal to the first ($y = 0, 1$) and one to last ($y = L - 2, L - 1$) unit cell of the 1D system. The projection operator onto the absorbing terminals,

$$P = \begin{cases} 1, & \text{if } y \in \{0, 1, L - 2, L - 1\}, \\ 0, & \text{otherwise.} \end{cases} \quad (3)$$

is of size $4 \times L$ or $8 \times 2L$, depending on whether the waveguides probing the HOTI are attached only to the last sites (as in Fig. 2a,b,c), or to the full unit cell (as in Fig. 2d). Transmission $\tilde{t}^{(l)}$ and reflection $\tilde{r}^{(l)}$ from the two absorbing terminals at the ends of the 1D system can be computed from the nested scattering matrix³

$$\tilde{S}(\phi) = P[1 - e^{i\phi}r(1 - P^T P)]^{-1}e^{i\phi}rP^T \quad (4)$$

having the same block structure as Eq. (2). The interpretation of Eq. (4) in Floquet language is as follows: it corresponds to an infinite sum over different scattering processes, obtained by expanding the inverse in a geometric series. Each successive term describes time-evolution over an additional period, obtained by applying the ‘Floquet operator’ r . Each state is projected out if it reaches the absorbing terminals (given by P) and continues evolving for another driving cycle if it does not overlap with the terminals (given by $1 - P^T P$). The nested scattering matrix \tilde{S} inherits particle-hole symmetry from the reflection block of the scattering matrix S . Indeed, $r = \tau_z r^* \tau_z$ together with Eq. (4) imply $\tilde{r}(\phi) = \tau_z \tilde{r}^*(-\phi) \tau_z$ [63]. As such,

³The equation is identical to that used in Refs. [63] to study driven systems, with the exception that the Floquet operator \mathcal{F} has been replaced by r , and its quasi-energies ε have been replaced by the phases ϕ .

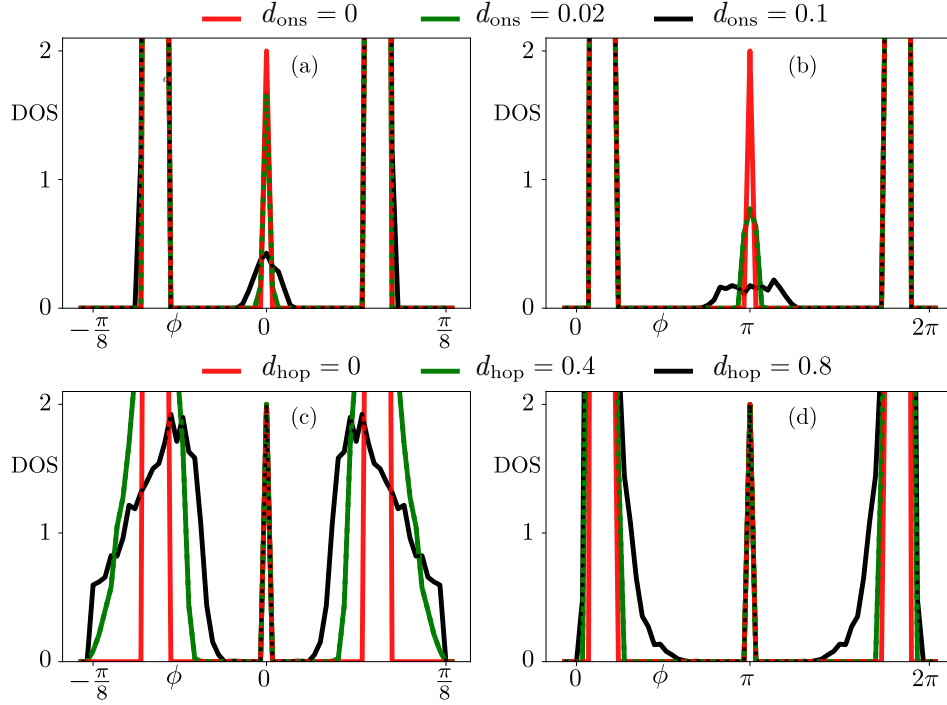


Figure 3: The evolution of the DOS (of the reflection matrix) with disorder. For every disorder realization, we calculate the DOS by dividing the full eigenphase range into 60 equally sized intervals. Panels (a) and (b) concern onsite disorder, while panels (c) and (d) reveal effects of randomness in hopping strengths. In panels (a) and (c), we consider a reflection matrix with 0-modes ($\gamma_x = 1.2, \gamma_y = 0.4, \lambda_x = \lambda_y = 1$), while panels (b) and (d) show how disorder influences a reflection matrix with only π -modes ($\gamma_x = \gamma_y = 0.4, \lambda_x = \lambda_y = 1$). In all cases, the system size is 60×60 sites.

the determinants of $\tilde{r}(\phi = 0)$ and $\tilde{r}(\phi = \pi)$ are real and the topological invariants are given by

$$\nu^0 = \text{sign det}[\tilde{r}(0)], \quad \nu^\pi = \text{sign det}[\tilde{r}(\pi)], \quad (5)$$

see also [60, 67, 68, 79, 80]. We have checked that the two \mathbb{Z}_2 indices correctly capture the presence of topological modes in the spectrum of r . Whenever there are mid-gap modes at $\phi = 0$ or $\phi = \pi$, we find that ν^0 or ν^π take the nontrivial value -1 . Otherwise, they take the trivial value $+1$. In Appendix C, we show how changing the HOTI parameters leads to topological phase transitions of the reflection matrix, signaled by changes in its topological invariants. These phase transitions can occur both by preserving the unitarity of r (the 2D HOTI remains insulating), or by rendering it singular (the 2D HOTI conducts).

5 Disorder effects

Systems with gapless corner modes have successfully been realized in many different platforms [35–50], most of them being the classical analogs of condensed matter systems. Even though such realizations offer a better control over disorder, its complete elimination remains

a challenging task. For this reason, we consider two types of imperfections in the 2D system. One kind of disorder breaks the particle-hole symmetry, while the other one preserves it. In the following, we will study how these disorder types affect topological phases of the reflection matrix.

Disorder which breaks \mathcal{P} is simulated by means of random onsite energies, drawn independently for every site from the uniform distribution on $[-d_{\text{ons}}, d_{\text{ons}}]$. Here, d_{ons} denotes the strength of disorder. Disorder which preserves \mathcal{P} is modeled with $\gamma_{x(y)} \rightarrow \gamma_{x(y)} + \delta_{\text{hop}}$ and $\lambda_{x(y)} \rightarrow \lambda_{x(y)} + \delta_{\text{hop}}$, where δ_{hop} drawn independently for each hopping from the uniform distribution on $[-d_{\text{hop}}, d_{\text{hop}}]$, where d_{hop} represents disorder strength. For both situations, we consider 250 disorder realizations and study averaged density of states (DOS) of the eigenphases of the reflection matrix. The results for phases with 0-modes and π -modes are given in Fig. 3.

The effect of the onsite disorder that breaks \mathcal{P} on 0-modes and π -modes is shown in Fig. 3a and Fig. 3b, respectively. We expect this type of disorder to shift the eigenphases of end modes from the particle-hole (and chiral) invariant points of the ϕ -spectrum, thus diminishing the DOS peak at $\phi = 0, \pi$. This effect is noticeable in both panels, and even for very small disorder strengths. Further increase of the disorder strength pushes eigenphases of these end states (at $\phi = 0, \pi$ in the clean limit) towards the bulk values, after which the DOS midgap peak disappears. Finally, even though π -modes are related to gapless Hamiltonian states, while 0-modes are not, both kinds are similarly affected by disorder. This is because the existence of both kinds of states originates from symmetry requirements on r .

On the other side, we expect the nontrivial phase of the reflection matrix to be more stable to spatial disorder that preserves \mathcal{P} . From the perspective of the 2D system, this type of disorder cannot move corner states from zero-energy but it reduces the bulk mobility gap. Once a mobility gap closing occurs, the reflection matrix loses unitarity, and cannot be used to simulate Floquet phases of Hermitian systems. For this reason, we restrict ourselves to disorder strengths which leave r unitary for every disorder realization with $1 - |\det r| \leq 10^{-6}$. As randomness in hoppings preserves \mathcal{P} , 0-modes and π -modes remain pinned to $\phi = 0, \pi$ as observed in Fig. 3c and in Fig. 3d, respectively.

6 Experimental feasibility

Our insight that a static system which is weakly probed simulates a Floquet system opens an alternate route to the experimental realization of Floquet topological phases. The method relies on two parts: (1) constructing a HOTI and (2) measuring the eigenphases of its reflection matrix. The first part has already been achieved in photonic [35–37], phononic [38], microwave [39], acoustic [41–47, 50], topoelectric [40], and condensed-matter [49] metamaterials, producing HOTI Hamiltonians similar to Eq. (1). Many of these platforms also allow to directly measure the phase of reflected waves, either by means of interferometry, as done in microwave [51], photonic [52], acoustic [81], and topoelectric [82] systems, or by directly visualizing the standing wave pattern formed at the sample boundary, as done, e.g., with electronic [49] or water waves [53]. Indeed, the authors of [49] have recently reported experiments realizing a HOTI by placing impurities on a surface in a Kagome lattice and measuring the system using scanning tunneling microscopy. While the focus of their paper is on the system itself, their Fig. 2 clearly shows a standing wave pattern of electronic waves reflected from the

system boundary. Our prediction is that extracting the reflection matrix eigenphases from this pattern will yield gapped bands and topological mid-gap states. Note that these static HOTI systems even allow to simulate the stroboscopic time-evolution of Floquet topological phases, as the reflection matrix r of the static system is exactly the stroboscopic evolution operator. Reflecting incoming waves off a HOTI system thus emulates the evolution over a single period. In order to simulate a periodic driving over multiple time periods, our setup has to be altered such that the incoming wave undergoes multiple subsequent scattering processes.

7 Conclusion

We have introduced a dimensional reduction procedure based on the scattering matrix, which maps the 2D Hamiltonian of a HOTI into the 1D Floquet operator of a nontrivial chain. Based on our insight that the reflection matrix can simulate a Floquet operator, we have shown that the topological invariants of the former can be obtained by defining nested scattering matrices. Moreover, our results provide an experimentally accessible route to simulate and measure the properties of Floquet systems, one which does not suffer from noise-induced decoherence.

Our work opens several directions for further research. First, the dimensional reduction scheme we have introduced can be adapted to other symmetry classes, as well as to reflection matrices which inherit lattice symmetries, such as mirror, rotation, and glide, from the parent HOTI. Building on our work, we anticipate that a link between the classifications of static and driven topological phases can also be established in these systems. Moreover, in three-dimensional HOTIs with corner states, recently realized in acoustic [44–47] and topoelectric [48] metamaterials, we expect the reflection matrix to exhibit corner states of its own, thus simulating a Floquet HOTI. For three-dimensional systems, it would be interesting to successively apply the nested scattering matrix construction twice. Furthermore, for HOTIs where only two of the four corners show zero modes [83–86], the reflection matrix from one side may show an odd number of topological states, thus simulating a Floquet system which falls outside of the existing, ‘tenfold way’ [87] classification of topological phases.

Acknowledgments

We thank Mikael Rechtsman for useful discussions and Ulrike Nitzsche for technical assistance.

Author contributions F.H. and I.C.F. initiated and oversaw the project. S.F. carried out the analysis of the reflection matrix, wrote the code, and performed numerical calculations. S.F. and I.C.F. produced the figures. All authors contributed to formulating the results and writing the manuscript.

Funding information This work is supported by the Deutsche Forschungsgemeinschaft (DFG, German Research Foundation) through the Würzburg-Dresden Cluster of Excellence on Complexity and Topology in Quantum Matter – *ct.qmat* (EXC 2147, project-id 39085490) and under Germany’s Excellence Strategy – Cluster of Excellence Matter and Light for Quantum Computing (ML4Q) EXC 2004/1 390534769.

A Calculating the reflection matrix

Our starting point is the 2D real-space Hamiltonian corresponding to Eq. (1) of the main text. We define two translationally invariant leads along the x -direction, where each lead is modeled as an array of isolated waveguides arranged such that each chain connects to only one site of the system. To compute the scattering matrix, we solve the Schrödinger equation [68, 70]

$$(H - E)(\psi_n^{\text{in}} + \sum_m S_{mn} \psi_m^{\text{out}} + \psi^{\text{loc}}) = 0 \quad (6)$$

corresponding to the full, system-plus-leads tight-binding model, described by the Hamiltonian H . Here, E denotes the Hamiltonian eigenvalues, ψ^{loc} stands for wave-functions which are localized in and near the scattering region, and $\psi_n^{\text{in/out}}$ denote incoming and outgoing lead states, that is, plane waves with velocity pointing towards or away from the system, respectively. For detecting states at zero energy, one takes $E = 0$ in the above calculation. The scattering matrix S with elements S_{mn} is obtained directly from the solution of the above equation. All our simulations are done using kwant [70].

In the two terminal geometry, S is a 2×2 block matrix in which the diagonal blocks are reflection matrices, and the off-diagonal blocks are transmission matrices. We are interested in the regime where the transmission between leads vanishes, yielding unitary reflection matrices r and r' . If we construct spinors $\Psi_{L/R}^{\text{in/out}}$ containing all incoming and outgoing modes in both the left (L) and right (R) leads, then we obtain

$$\Psi_L^{\text{out}} = r \Psi_L^{\text{in}} \quad (7)$$

for the reflection matrix of the left lead r . The last relation becomes an eigenvalue equation for $\Psi_L^{\text{out}} = e^{i\phi} \Psi_L^{\text{in}}$, implying that the eigenmodes of reflection matrix are standing waves formed as superpositions of Ψ_L^{in} and Ψ_L^{out} . The spectrum of the reflection matrix, consisting of the eigenphases ϕ , influences the standing wave pattern formed at the sample boundary.

B Symmetries of the reflection matrix

The Hamiltonian H is particle-hole and chiral symmetric, with operators $\mathcal{P} = \tau_z \mathcal{K}$ and $\mathcal{C} = \tau_z$, respectively. We study how these symmetries constrain S by using the Schrödinger equation Eq. (6). The procedure has been detailed in Ref. [68] for local symmetries, and relies on knowing how they affect Hamiltonian and incoming/outgoing modes. For this reason, we skip the derivation, and give below the relations corresponding to particle-hole and chiral symmetry, respectively. The reflection matrix obeys

$$U_{\mathcal{P}} r^* U_{\mathcal{P}}^\dagger = r, \quad U_{\mathcal{C}} r^\dagger U_{\mathcal{C}}^\dagger = r, \quad (8)$$

where $U_{\mathcal{P}} = U_{\mathcal{C}} = \tau_z$. Both expressions provide the same constraint on the determinant of r as

$$\det r^* = \det r, \quad (9)$$

due to the fact that $\det (r^*)^T = \det r^*$. Hence, in both cases, eigenvalue spectra of r consists of complex-conjugate pairs and real values ± 1 .

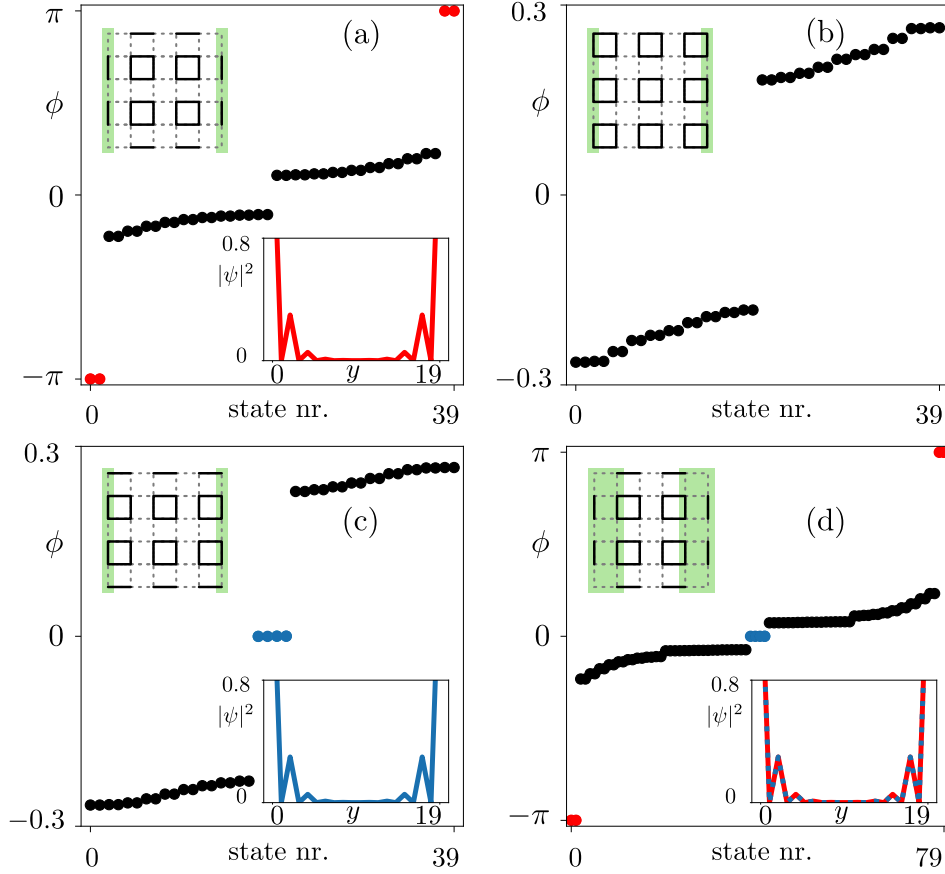


Figure 4: Eigenphases of the reflection matrix, showing π -modes (0-modes) and their associated wavefunctions in red (blue). We consider a bilayer of HOTI systems, each with 20×20 sites. In all panels, $\lambda_{x,y} = 1$ and $D_x = D_y = 0.15$. We have chosen $\gamma_{x,y} = 0.4$ in panels (a) and (d), $\gamma_{x,y} = 1.2$ in panel (b), whereas $\gamma_x = 1.2$ and $\gamma_y = 0.4$ in panel (c). Insets sketch the corresponding dimerization pattern of the HOTI as well as the sites connected to the lead (green). The system-lead coupling strength is $t_{sl} = 0.5$ in all cases.

It is known that a unitary 1D system with $0/\pi$ -modes protected by \mathcal{P} follows a $\mathbb{Z}_2 \times \mathbb{Z}_2$ classification, while a $\mathbb{Z} \times \mathbb{Z}$ classification occurs in 1D systems where \mathcal{C} is the protecting symmetry [14]. To find scattering invariants of a 1D system described by r , we calculate the reflection matrix $\tilde{r}(\phi = 0, \pi)$ of one end of this system [63]. For systems with \mathcal{P} , the invariant $\text{sign det}[\tilde{r}(\phi = 0, \pi)]$ takes only two values, -1 for a system with topologically protected modes and 1 otherwise. In chiral symmetric phases, the invariant is the number of negative eigenvalues $\nu_n[\tilde{r}(\phi = 0, \pi)]$ in the basis where \tilde{r} is Hermitian [68].

In the phase with a single π -mode per end, $\tilde{r}(\phi = \pi)$ is a 2×2 matrix with $\det[\tilde{r}(\pi)] = -1$. This implies the spectrum of $\tilde{r}(\pi)$ has to be real, and the chiral invariant reads $\nu_n[\tilde{r}(\pi)] = 1$. Both invariants are thus in agreement. In the phase with a 0-mode at each end, we obtain the same values of invariants for $\phi = 0$. Finally, in the anomalous phase, $\tilde{r}(\phi = 0, \pi)$ is a unitary 4×4 matrix with negative determinant. We transform to the basis in which \tilde{r} is Hermitian via $\tilde{r} \mapsto U\tilde{r}U^\dagger$, $U = \text{diag}(i, 1) \otimes \sigma_0$, and we again obtain $\nu_n[\tilde{r}(\phi = 0, \pi)] = 1$.

For the phases described in the main text, both \mathcal{P} and \mathcal{C} protect only one 0- and/or π -

mode per end. However, by considering two copies of the 2D HOTI system and coupling them in a way that preserves local symmetries, one can obtain a reflection matrix with two modes per end. The momentum-space Hamiltonian for this bilayer system reads

$$H_{\text{bilayer}}(\mathbf{k}) = h(\mathbf{k})\eta_0 + D_x\tau_y\sigma_z\eta_y + D_y\tau_x\sigma_y\eta_y \quad (10)$$

where $h(\mathbf{k})$ is the Hamiltonian Eq. (1) of the main text. D_x and D_y denote intralayer couplings, while the additional layer degree of freedom is represented by Pauli matrices η . Here, for simplicity, we assumed intralayer hoppings are momentum independent, i.e., they only connect sites within the unit cell. The chiral symmetry operator reads $\mathcal{C} = \tau_z\sigma_0\eta_0\mathcal{K}$. The calculated reflection matrix spectra for different parameters is plotted in Fig. 4.

In Fig. 4a, the eigenphase spectra calculated for a bilayer system in the HOTI phase reveals the presence of four π -modes. They form two pairs, each pair pinned to an end, as shown in the lower inset. Dimerizing a bilayer system trivially in both directions results in a trivial Floquet phase, see Fig. 4b. Furthermore, if the system is nontrivial only in the y -direction, the eigenphase spectrum of r contains four 0-modes, as seen in Fig. 4c. Finally, attaching leads to a full unit cell on the boundary gives an anomalous phase whose spectra is plotted in Fig. 4d. The number of negative eigenvalues of \tilde{r} differs by 2 across the phase transition between trivial and topological phases. For example, the topological phase of a 1D system with π -modes is described by $\nu_n[\tilde{r}(\phi = \pi)] = 2$ indicating $\nu^\pi = 1$. Therefore, in the bilayer case, the particle-hole invariant cannot distinguish the topological from the trivial phase.

C Topological phase transitions of the reflection matrix

The gapless corner modes of a finite 2D system in a HOTI phase, described by the Hamiltonian Eq. (1) of the main text, can depart from zero energy as a result of various gap closings. Some of these phase transitions occur only on the edges, like the x -edge gap closing that appears when $\gamma_x = \lambda_x$ and $\gamma_y \neq \lambda_y$ (and vice versa for the y -edge). The vanishing of an edge gap is related to the appearance of two counter-propagating modes per edge that are protected by translation symmetry [88–90]. Furthermore, a bulk gap closing occurs for $\gamma_x = \gamma_y = \lambda_x = \lambda_y$ at $(k_x, k_y) = (\pi, \pi)$. These phase transitions affect the reflection matrix r that describes the left edge of the 2D system.

First, we study the topological phase transition of r induced by a y -edge gap closing of the 2D system. Here, r remains unitary across the phase transition, provided the HOTI remains insulating in the x direction. Thus, the spectrum of r lies on the unit circle, and henceforth only its eigenphase (ϕ) spectrum is plotted. For a finite 2D system, ϕ -spectrum can have topologically protected states at particle-hole invariant eigenphases, as shown in Fig. 2 of the main text. In this case, the nested scattering matrix topological invariants ν^0 and ν^π can be used to study the phase transition. Here, we consider instead results obtained in a ribbon geometry, for which the HOTI is infinite along the y direction, such that the momentum k_y is a good quantum number. The dispersion of the reflection matrix, $\phi(k_y)$, is shown in Fig. 5 for different values of γ_y/λ_y , while keeping $\gamma_x/\lambda_x < 1$. In this ribbon geometry r is a 2×2 matrix and its eigenphases form two bands. In Fig. 5a the bands are plotted for a system in a HOTI phase. For the same parameters, the ϕ -spectrum of an open 1D system has π -modes (see Fig. 2a of the main text). For $\gamma_y = \lambda_y$ a band gap closing occurs at $\phi = \pi$, thus signaling the hybridization of two π -modes and their shift into the bulk of the 1D unitary system. Finally,

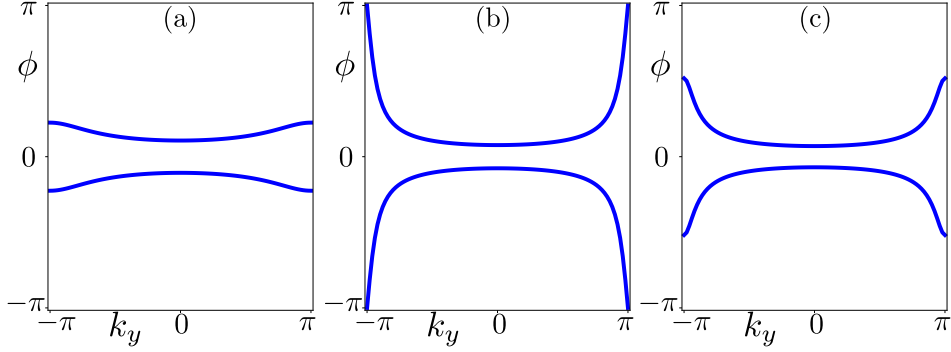


Figure 5: The dispersion $\phi(k_y)$ of the 2×2 matrix r is calculated across the phase transition related to the y -edge gap closing of the 2D system. In all panels $\lambda_x = \lambda_y = 1$, and there are 36 sites in the x -direction. In panel (a), the 2D system is in a HOTI phase with $\gamma_x = \gamma_y = 0.4$. The intracell hoppings for panel (b) are $\gamma_x = 0.4$ and $\gamma_y = 1$, and in panel (c) $\gamma_x = 0.4$ and $\gamma_y = 1.2$. The band gap closing at $\phi = \pi$ signals the disappearance of π -modes in the ϕ -spectrum corresponding to the reflection matrix of a finite 2D system.

Fig. 5c corresponds to $\gamma_y > \lambda_y$, and shows again two gapped bands. As in Floquet systems, the phase transition of r is accompanied by a gap closing and reopening.

In a similar fashion, one can also study the phase transition between the phase that supports 0-modes and a trivial phase. Then, the dispersion of r would show a band gap closing at $\phi = 0$ for $\gamma_y = \lambda_y$. Finally, r that simulates an anomalous Floquet phase is obtained by attaching lead to a unit cell of sites, and is thus a 4×4 matrix in the k_y -space. The phase transition in this case would involve four bands that cross at both 0- and π -eigenphases for $\gamma_y = \lambda_y$.

Phase transitions which preserve the unitarity of r can be studied from the perspective of its \mathbb{Z}_2 topological invariants $\nu^{0(\pi)}$. By definition, these invariants are discontinuous at the phase transition point, and match the value of $\det[\tilde{r}(\phi = 0, \pi)]$ sufficiently far from it. Thus, in Fig. 6, we plot the dependence of $\det[\tilde{r}(\phi = 0, \pi)]$ on dimerization in the y -direction. In Fig. 6a, we start from a system initially dimerized such that r describes a 1D system with π -modes, hence $\det[\tilde{r}(\pi)] = -1$ and $\det[\tilde{r}(0)] = 1$. The latter quantity does not change across the phase transition, while $\gamma_y/\lambda_y \rightarrow 1$ implies $\det[\tilde{r}(\pi)] = 0$. The nested reflection matrix \tilde{r} has a zero eigenvalue due to the conducting y -edge [67], while for $\gamma_y > \lambda_y$, $\det[\tilde{r}(\pi)] = 1$. Fig. 6b describes a similar situation, as now we start from a system with 0-modes, and therefore $\det[\tilde{r}(0)]$ changes the value from -1 to 1 across the phase transition. If r describes an anomalous Floquet phase, increasing γ_y/λ_y causes both $\det[\tilde{r}(0)]$ and $\det[\tilde{r}(\pi)]$ to change values from -1 to 1 , as seen in Fig. 6c.

In the case of an x -edge or a bulk gap closing, the finite transmission between the leads renders r subunitary. This implies that not all complex eigenvalues z of r have $|z| = 1$, so not all information is encoded in their phase. Thus, we study these phase transitions by plotting z in the complex plane $(\text{Re}(z), \text{Im}(z))$, like in Fig. 7. For r calculated with open boundary conditions in the y -direction, these eigenvalues are represented by black dots. If however, we have a finite system with a periodic boundary condition (PBC) in the y -direction, z 's are represented by light blue crosses. To visually identify eigenvalues with $|z| = 1$, we always plot a unit circle, colored in grey.

Due to the weak link (hopping strength t_{sl}) between the system and the lead (with hopping

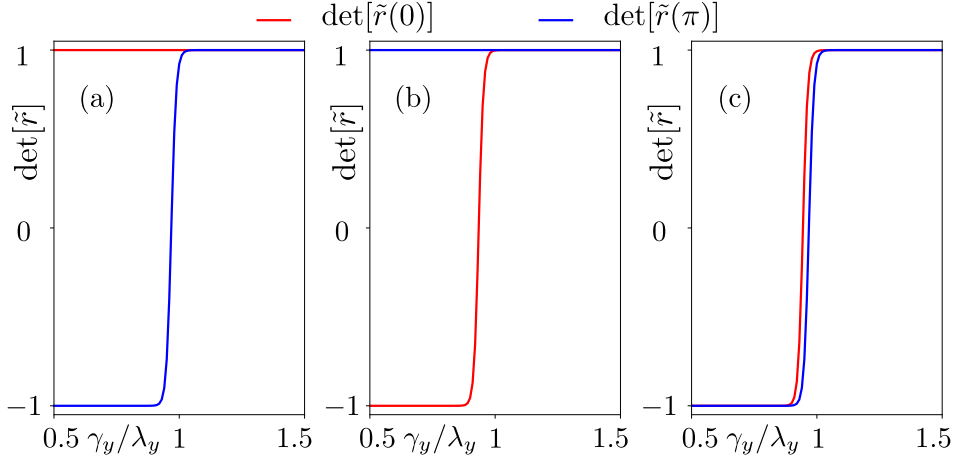


Figure 6: The dependence of $\det[\tilde{r}]$ at eigenphases $\phi = 0, \pi$ on the ratio γ_y/λ_y , with $\lambda_x = \lambda_y = 1$. In panels (a) and (b) we use $\gamma_x = 0.4$ and $\gamma_x = 1.2$, respectively, and r is obtained by attaching leads only to the sites closest to the boundary of the 2D HOTI. In panel (c) however, r is calculated for leads attached to the full unit cell of the 2D system, while the parameters are the same as in panel (a). In all panels, the 2D system consists of 100×100 sites and it is connected to leads with hopping strength $t_{\text{lead}} = 1$ via a weak link with hopping strength $t_{\text{sl}} = 0.5$.

t_{lead}), translation symmetry is broken at the system-lead interface. The weak link causes back-scattering of the gapless edge and bulk states present in the 2D system at its phase transitions. As such, $\det r = 0$, which would correspond to perfect transmission, does not exactly coincide with gap closings of the 2D system. Rather, $\det r = 0$ for $\gamma_x/\lambda_x = 1 - \delta$, with $\delta > 0$, where δ is a function of t_{sl} . This explains why in Fig. 7 the zero eigenvalues of the reflection matrix do not occur exactly at $\gamma_x = 1$, but are shifted closer to the value $\gamma_x = 0.925$.

We start with a unitary r whose ϕ -spectrum has two π -modes denoted by red color in Fig. 7a. As γ_x increases (while keeping γ_y/λ_y constant), these boundary modes shift along the x -axis. For an appropriate δ , they are located exactly at $(\text{Re}(z), \text{Im}(z)) = (0, 0)$ and $\det r = 0$ (see Fig. 7b). By further increasing γ_x/λ_x , these modes move along the horizontal axis to become 0-modes, colored in dark blue in Fig. 7c. Meanwhile, the r eigenvalues calculated in the presence of a PBC remain on the unit circle, as gapless counter-propagating modes on opposite edges are now coupled.

In the proximity of a bulk gap closing, r has a phase transition between a topological and a trivial phase. To study the latter, we start from r with two π -modes, whose spectrum is plotted in Fig. 7d. As the system approaches the phase transition point, these modes split into a complex-conjugate pair that does not lie on the unit circle, as seen in Fig. 7e. This is because the system conducts but not with a unit conductance due to finite size energy splittings. Finite size effects are eliminated upon the introduction of PBC, as we see two bulk modes at $(\text{Re}(z), \text{Im}(z)) = (0, 0)$ in Fig. 7e. Increasing intracell hoppings with respect to intercell ones moves all modes back to the unit circle. We see in Fig. 7f that r now describes a trivial system.

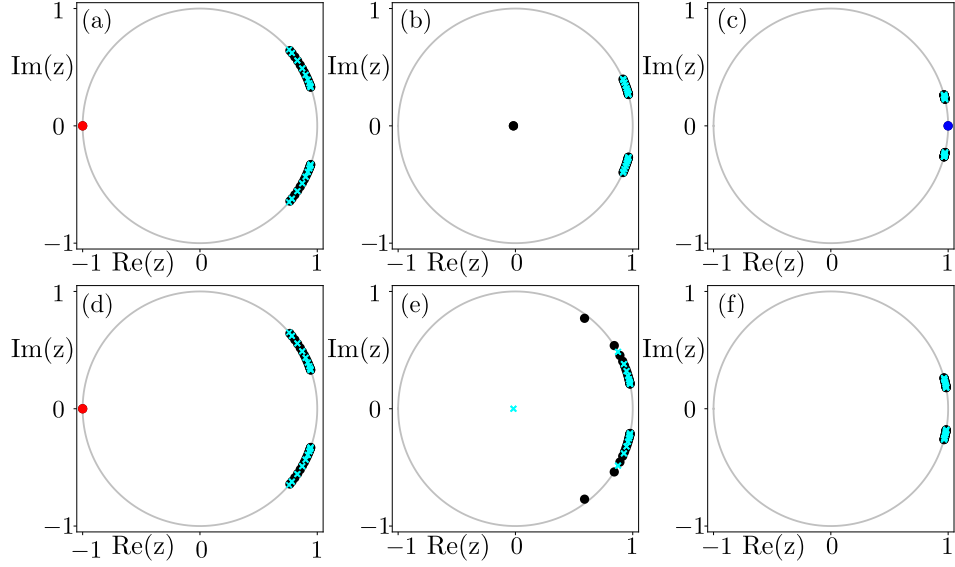


Figure 7: Eigenvalues of r (called z) are represented in the complex plane ($\text{Re}(z)$, $\text{Im}(z)$). The matrix r is calculated for a system made of 36×36 sites. The spectrum of an open system is denoted by black dots, while light blue crosses represent the spectrum in the presence of a periodic boundary condition in the y direction. We always take $\lambda_x = \lambda_y = 1$, and panels (a) and (d) are calculated for $\gamma_x = \gamma_y = 0.4$. Red and dark blue dots correspond to π -modes and 0-modes, respectively, of the ϕ -spectrum. Panels (b) and (c) have the same $\gamma_y = 0.4$ and differ in $\gamma_x = 0.925$ and $\gamma_x = 1.2$, respectively. Intracell hoppings in panel (e) are $\gamma_x = 0.925$ and $\gamma_y = 1$, while $\gamma_x = \gamma_y = 1.2$ in panel (f). As in Fig. 6, we take $t_{\text{lead}} = 1$ and $t_{\text{sl}} = 0.5$ for all panels.

References

- [1] M. Z. Hasan and C. L. Kane, *Colloquium: Topological insulators*, Rev. Mod. Phys. **82**, 3045 (2010), doi:10.1103/RevModPhys.82.3045.
- [2] X.-L. Qi and S.-C. Zhang, *Topological insulators and superconductors*, Rev. Mod. Phys. **83**, 1057 (2011), doi:10.1103/RevModPhys.83.1057.
- [3] T. Kitagawa, E. Berg, M. Rudner and E. Demler, *Topological characterization of periodically driven quantum systems*, Phys. Rev. B **82**, 235114 (2010), doi:10.1103/PhysRevB.82.235114.
- [4] A. Gómez-León and G. Platero, *Floquet-Bloch theory and topology in periodically driven lattices*, Phys. Rev. Lett. **110**, 200403 (2013), doi:10.1103/PhysRevLett.110.200403.
- [5] A. P. Schnyder, S. Ryu, A. Furusaki and A. W. W. Ludwig, *Classification of topological insulators and superconductors*, AIP Conf. Proc. **1134**, 10 (2009), doi:10.1063/1.3149481.
- [6] A. Kitaev, *Periodic table for topological insulators and superconductors*, AIP Conf. Proc. **1134**, 22 (2009), doi:10.1063/1.3149495.

- [7] S. Ryu, A. P. Schnyder, A. Furusaki and A. W. W. Ludwig, *Topological insulators and superconductors: tenfold way and dimensional hierarchy*, *New J. Phys.* **12**, 065010 (2010), doi:10.1088/1367-2630/12/6/065010.
- [8] C.-K. Chiu, H. Yao and S. Ryu, *Classification of topological insulators and superconductors in the presence of reflection symmetry*, *Phys. Rev. B* **88**, 075142 (2013), doi:10.1103/PhysRevB.88.075142.
- [9] M. S. Rudner, N. H. Lindner, E. Berg and M. Levin, *Anomalous edge states and the bulk-edge correspondence for periodically driven two-dimensional systems*, *Phys. Rev. X* **3**, 031005 (2013), doi:10.1103/PhysRevX.3.031005.
- [10] K. Shiozaki and M. Sato, *Topology of crystalline insulators and superconductors*, *Phys. Rev. B* **90**, 165114 (2014), doi:10.1103/PhysRevB.90.165114.
- [11] C.-K. Chiu, J. C. Y. Teo, A. P. Schnyder and S. Ryu, *Classification of topological quantum matter with symmetries*, *Rev. Mod. Phys.* **88**, 035005 (2016), doi:10.1103/RevModPhys.88.035005.
- [12] F. Nathan and M. S. Rudner, *Topological singularities and the general classification of Floquet–Bloch systems*, *New J. Phys.* **17**, 125014 (2015), doi:10.1088/1367-2630/17/12/125014.
- [13] D. V. Else and C. Nayak, *Classification of topological phases in periodically driven interacting systems*, *Phys. Rev. B* **93**, 201103(R) (2016), doi:10.1103/PhysRevB.93.201103.
- [14] R. Roy and F. Harper, *Periodic table for Floquet topological insulators*, *Phys. Rev. B* **96**, 155118 (2017), doi:10.1103/PhysRevB.96.155118.
- [15] S. Yao, Z. Yan and Z. Wang, *Topological invariants of Floquet systems: General formulation, special properties, and Floquet topological defects*, *Phys. Rev. B* **96**, 195303 (2017), doi:10.1103/PhysRevB.96.195303.
- [16] J. Kruthoff, J. de Boer, J. van Wezel, C. L. Kane and R.-J. Slager, *Topological classification of crystalline insulators through band structure combinatorics*, *Phys. Rev. X* **7**, 041069 (2017), doi:10.1103/PhysRevX.7.041069.
- [17] H. Po, A. Vishwanath and H. Watanabe, *Symmetry-based indicators of band topology in the 230 space groups*, *Nat. Commun.* **8**, 50 (2017), doi:10.1038/s41467-017-00133-2.
- [18] B. Bradlyn, L. Elcoro, J. Cano, M. G. Vergniory, Z. Wang, C. Felser, M. I. Aroyo and B. A. Bernevig, *Topological quantum chemistry*, *Nature* **547**, 298–305 (2017), doi:10.1038/nature23268.
- [19] T. Zhang, Y. Jiang, Z. Song, H. Huang, Y. He, Z. Fang, H. Weng and C. Fang, *Catalogue of topological electronic materials*, *Nature* **566**, 475–479 (2019), doi:10.1038/s41586-019-0944-6.
- [20] M. G. Vergniory, L. Elcoro, C. Felser, N. Regnault, B. A. Bernevig and Z. Wang, *A complete catalogue of high-quality topological materials*, *Nature* **566**, 480–485 (2019), doi:10.1038/s41586-019-0954-4.

- [21] F. Tang, H. C. Po, A. Vishwanath and X. Wan, *Comprehensive search for topological materials using symmetry indicators*, Nature **566**, 486–489 (2019), doi:10.1038/s41586-019-0937-5.
- [22] Z.-D. Song, L. Elcoro, Y.-F. Xu, N. Regnault and B. A. Bernevig, *Fragile phases as affine monoids: Classification and material examples*, Phys. Rev. X **10**, 031001 (2020), doi:10.1103/PhysRevX.10.031001.
- [23] L. D’Alessio and M. Rigol, *Long-time behavior of isolated periodically driven interacting lattice systems*, Phys. Rev. X **4**, 041048 (2014), doi:10.1103/PhysRevX.4.041048.
- [24] A. Lazarides, A. Das and R. Moessner, *Equilibrium states of generic quantum systems subject to periodic driving*, Phys. Rev. E **90**, 012110 (2014), doi:10.1103/PhysRevE.90.012110.
- [25] T. Groh, S. Brakhane, W. Alt, D. Meschede, J. K. Asbóth and A. Alberti, *Robustness of topologically protected edge states in quantum walk experiments with neutral atoms*, Phys. Rev. A **94**, 013620 (2016), doi:10.1103/PhysRevA.94.013620.
- [26] M.-T. Rieder, L. M. Sieberer, M. H. Fischer and I. C. Fulga, *Localization counteracts decoherence in noisy Floquet topological chains*, Phys. Rev. Lett. **120**, 216801 (2018), doi:10.1103/PhysRevLett.120.216801.
- [27] L. M. Sieberer, M.-T. Rieder, M. H. Fischer and I. C. Fulga, *Statistical periodicity in driven quantum systems: General formalism and application to noisy Floquet topological chains*, Phys. Rev. B **98**, 214301 (2018), doi:10.1103/PhysRevB.98.214301.
- [28] W. A. Benalcazar, B. A. Bernevig and T. L. Hughes, *Quantized electric multipole insulators*, Science **357**(6346), 61–66 (2017), doi:10.1126/science.aah6442.
- [29] W. A. Benalcazar, B. A. Bernevig and T. L. Hughes, *Electric multipole moments, topological multipole moment pumping, and chiral hinge states in crystalline insulators*, Phys. Rev. B **96**, 245115 (2017), doi:10.1103/PhysRevB.96.245115.
- [30] F. Schindler, A. M. Cook, M. G. Vergniory, Z. Wang, S. S. P. Parkin, B. A. Bernevig and T. Neupert, *Higher-order topological insulators*, Sci. Adv. **4**, 0346 (2018), doi:10.1126/sciadv.aat0346.
- [31] F. Schindler, Z. Wang, M. G. Vergniory, A. M. Cook, A. Murani, S. Sengupta, A. Y. Kasumov, R. Deblock, S. Jeon, I. Drozdov, H. Bouchiat, S. Guéron *et al.*, *Higher-order topology in bismuth*, Nature Physics **14**, 918–924 (2018), doi:10.1038/s41567-018-0224-7.
- [32] E. Khalaf, *Higher-order topological insulators and superconductors protected by inversion symmetry*, Phys. Rev. B **97**, 205136 (2018), doi:10.1103/PhysRevB.97.205136.
- [33] M. Geier, L. Trifunovic, M. Hoskam and P. W. Brouwer, *Second-order topological insulators and superconductors with an order-two crystalline symmetry*, Phys. Rev. B **97**, 205135 (2018), doi:10.1103/PhysRevB.97.205135.
- [34] L. Trifunovic and P. W. Brouwer, *Higher-order bulk-boundary correspondence for topological crystalline phases*, Phys. Rev. X **9**, 011012 (2019), doi:10.1103/PhysRevX.9.011012.

- [35] B.-Y. Xie, H.-F. Wang, H.-X. Wang, X.-Y. Zhu, J.-H. Jiang, M.-H. Lu and Y.-F. Chen, *Second-order photonic topological insulator with corner states*, Phys. Rev. B **98**, 205147 (2018), doi:10.1103/PhysRevB.98.205147.
- [36] B.-Y. Xie, G.-X. Su, H.-F. Wang, H. Su, X.-P. Shen, P. Zhan, M.-H. Lu, Z.-L. Wang and Y.-F. Chen, *Visualization of higher-order topological insulating phases in two-dimensional dielectric photonic crystals*, Phys. Rev. Lett. **122**, 233903 (2019), doi:10.1103/PhysRevLett.122.233903.
- [37] J. Noh, W. A. Benalcazar, S. Huang, M. J. Collins, K. P. Chen, T. L. Hughes and M. C. Rechtsman, *Topological protection of photonic mid-gap defect modes*, Nature Photonics **12**, 408–415 (2018), doi:10.1038/s41566-018-0179-3.
- [38] M. Serra-Garcia, V. Peri, R. Süsstrunk, O. R. Bilal, T. Larsen, L. G. Villanueva and S. D. Huber, *Observation of a phononic quadrupole topological insulator*, Nature **555**, 342–345 (2018), doi:10.1038/nature25156.
- [39] C. W. Peterson, W. A. Benalcazar, T. L. Hughes and G. Bahl, *A quantized microwave quadrupole insulator with topologically protected corner states*, Nature **555**, 346–350 (2018), doi:10.1038/nature25777.
- [40] S. Imhof, C. Berger, F. Bayer, J. Brehm, L. W. Molenkamp, T. Kiessling, F. Schindler, C. H. Lee, M. Greiter, T. Neupert and R. Thomale, *Topoelectrical-circuit realization of topological corner modes*, Nature Physics **14**, 925–929 (2018), doi:10.1038/s41567-018-0246-1.
- [41] H. Xue, Y. Yang, F. Gao, Y. Chong and B. Zhang, *Acoustic higher-order topological insulator on a Kagome lattice*, Nature Materials **18**, 108–112 (2018), doi:10.1038/s41563-018-0251-x.
- [42] X. Zhang, H.-X. Wang, Z.-K. Lin, Y. Tian, B. Xie, M.-H. Lu, Y.-F. Chen and J.-H. Jiang, *Second-order topology and multidimensional topological transitions in sonic crystals*, Nature Physics **15**, 582–588 (2019), doi:10.1038/s41567-019-0472-1.
- [43] Z.-G. Chen, C. Xu, R. Al Jahdali, J. Mei and Y. Wu, *Corner states in a second-order acoustic topological insulator as bound states in the continuum*, Phys. Rev. B **100**, 075120 (2019), doi:10.1103/PhysRevB.100.075120.
- [44] X. Zhang, B.-Y. Xie, H.-F. Wang, X. Xu, Y. Tian, J.-H. Jiang, M.-H. Lu and Y.-F. Chen, *Dimensional hierarchy of higher-order topology in three-dimensional sonic crystals*, Nat. Commun. **10**, 5331 (2019), doi:10.1038/s41467-019-13333-9.
- [45] H. Xue, Y. Yang, G. Liu, F. Gao, Y. Chong and B. Zhang, *Realization of an acoustic third-order topological insulator*, Phys. Rev. Lett. **122**, 245413 (2019), doi:10.1103/PhysRevLett.122.244301.
- [46] H. Xue, Y. Ge, H.-X. Sun, Q. Wang, D. Jia, Y.-J. Guan, S.-Q. Yuan, Y. Chong and B. Zhang, *Observation of an acoustic octupole topological insulator*, Nat. Commun. **11**, 2442 (2020), doi:10.1038/s41467-020-16350-1.

- [47] X. Ni, M. Li, M. Weiner, A. Alù and A. B. Khanikaev, *Demonstration of a quantized acoustic octupole topological insulator*, Nat. Commun. **11**, 2108 (2020), doi:10.1038/s41467-020-15705-y.
- [48] J. Bao, D. Zou, W. Zhang, W. He, H. Sun and X. Zhang, *Topoelectrical circuit octupole insulator with topologically protected corner states*, Phys. Rev. B **100**, 201406(R) (2019), doi:10.1103/PhysRevB.100.201406.
- [49] S. N. Kempkes, M. R. Slot, J. J. van den Broeke, P. Capiod, W. A. Benalcazar, D. Vanmaekelbergh, D. Bercioux, I. Swart and C. M. Smith, *Robust zero-energy modes in an electronic higher-order topological insulator*, Nature Materials **18**, 1292–1297 (2019), doi:10.1038/s41563-019-0483-4.
- [50] X. Zhang, Z.-K. Lin, H.-X. Wang, Z. Xiong, Y. Tian, M.-H. Lu, Y.-F. Chen and J.-H. Jiang, *Symmetry-protected hierarchy of anomalous multipole topological band gaps in nonsymmorphic metacrystals*, Nat. Commun. **11**, 65 (2020), doi:10.1038/s41467-019-13861-4.
- [51] W. Hu, J. C. Pillay, K. Wu, M. Pasek, P. P. Shum and Y. Chong, *Measurement of a topological edge invariant in a microwave network*, Phys. Rev. X **5** (2015), doi:10.1103/PhysRevX.5.011012.
- [52] Q. Wang, M. Xiao, H. Liu, S. Zhu and C. T. Chan, *Optical interface states protected by synthetic Weyl points*, Phys. Rev. X **7**, 031032 (2017), doi:10.1103/PhysRevX.7.031032.
- [53] N. Laforge, V. Laude, F. Chollet, A. Khelif, M. Kadic, Y. Guo and R. Fleury, *Observation of topological gravity-capillary waves in a water wave crystal*, New J. Phys. **21**, 083031 (2019), doi:10.1088/1367-2630/ab376a.
- [54] M. C. Rechtsman, J. M. Zeuner, Y. Plotnik, Y. Lumer, D. Podolsky, F. Dreisow, S. Nolte, M. Segev and A. Szameit, *Photonic Floquet topological insulators*, Nature **496**, 196–200 (2013), doi:10.1038/nature12066.
- [55] L. J. Maczewsky, J. M. Zeuner, S. Nolte and A. Szameit, *Observation of photonic anomalous Floquet topological insulators*, Nat. Commun. **8**, 13756 (2017), doi:10.1038/ncomms13756.
- [56] S. Mukherjee, A. Spracklen, M. Valiente, E. Andersson, P. Öhberg, N. Goldman and R. R. Thomson, *Experimental observation of anomalous topological edge modes in a slowly driven photonic lattice*, Nat. Commun. **8**, 13918 (2017), doi:10.1038/ncomms13918.
- [57] S. Mukherjee, H. K. Chandrasekharan, P. Öhberg, N. Goldman and R. R. Thomson, *State-recycling and time-resolved imaging in topological photonic lattices*, Nat. Commun. **9**, 4209 (2018), doi:10.1038/s41467-018-06723-y.
- [58] F. Cardano, A. D’Errico, A. Dauphin, M. Maffei, B. Piccirillo, C. de Lisio, G. D. Filippis, V. Cataudella, E. Santamato, L. Marrucci, M. Lewenstein and P. Massignan, *Detection of Zak phases and topological invariants in a chiral quantum walk of twisted photons*, Nat. Commun. **8**, 15516 (2017), doi:10.1038/ncomms15516.

- [59] K. Wang, X. Qiu, L. Xiao, X. Zhan, Z. Bian, W. Yi and P. Xue, *Simulating dynamic quantum phase transitions in photonic quantum walks*, Phys. Rev. Lett. **122**, 020501 (2019), doi:10.1103/PhysRevLett.122.020501.
- [60] A. Y. Kitaev, *Unpaired Majorana fermions in quantum wires*, Phys.-Usp. **44**, 131 (2001), doi:10.1070/1063-7869/44/10S/S29.
- [61] M. Thakurathi, A. A. Patel, D. Sen and A. Dutta, *Floquet generation of Majorana end modes and topological invariants*, Phys. Rev. B **88**, 155133 (2013), doi:10.1103/PhysRevB.88.155133.
- [62] M. Benito, A. Gómez-León, V. M. Bastidas, T. Brandes and G. Platero, *Floquet engineering of long-range p-wave superconductivity*, Phys. Rev. B **90**, 205127 (2014), doi:10.1103/PhysRevB.90.205127.
- [63] I. C. Fulga and M. Maksymenko, *Scattering matrix invariants of Floquet topological insulators*, Phys. Rev. B **93**, 075405 (2016), doi:10.1103/PhysRevB.93.075405.
- [64] Y. V. Fyodorov and H. J. Sommers, *Spectra of random contractions and scattering theory for discrete-time systems*, JETP Letters **72**, 422–426 (2000), doi:10.1134/1.1335121.
- [65] L. D. Landau and E. M. Lifshitz, *Quantum Mechanics: Non-Relativistic Theory*, Pergamon (1997).
- [66] I. A. Gruzberg, N. Read and S. Vishveshwara, *Localization in disordered superconducting wires with broken spin-rotation symmetry*, Phys. Rev. B **71**, 245124 (2005), doi:10.1103/PhysRevB.71.245124.
- [67] A. R. Akhmerov, J. P. Dahlhaus, F. Hassler, M. Wimmer and C. W. J. Beenakker, *Quantized conductance at the Majorana phase transition in a disordered superconducting wire*, Phys. Rev. Lett. **106**, 057001 (2011), doi:10.1103/PhysRevLett.106.057001.
- [68] I. C. Fulga, F. Hassler, A. R. Akhmerov and C. W. J. Beenakker, *Scattering formula for the topological quantum number of a disordered multimode wire*, Phys. Rev. B **83**, 155429 (2011), doi:10.1103/PhysRevB.83.155429.
- [69] W. P. Su, J. R. Schrieffer and A. J. Heeger, *Solitons in polyacetylene*, Phys. Rev. Lett. **42**, 1698 (1979), doi:10.1103/PhysRevLett.42.1698.
- [70] C. W. Groth, M. Wimmer, A. R. Akhmerov and X. Waintal, *Kwant: a software package for quantum transport*, New J. Phys. **16**, 063065 (2014), doi:10.1088/1367-2630/16/6/063065.
- [71] I. C. Fulga, F. Hassler and A. R. Akhmerov, *Scattering theory of topological insulators and superconductors*, Phys. Rev. B **85**, 165409 (2012), doi:10.1103/PhysRevB.85.165409.
- [72] L. Jiang, T. Kitagawa, J. Alicea, A. R. Akhmerov, D. Pekker, G. Refael, J. I. Cirac, E. Demler, M. D. Lukin and P. Zoller, *Majorana fermions in equilibrium and in driven cold-atom quantum wires*, Phys. Rev. Lett. **106**, 220402 (2011), doi:10.1103/PhysRevLett.106.220402.

- [73] M. Rodriguez-Vega, A. Kumar and B. Seradjeh, *Higher-order Floquet topological phases with corner and bulk bound states*, Phys. Rev. B **100**, 085138 (2019), doi:10.1103/PhysRevB.100.085138.
- [74] R. W. Bomantara, L. Zhou, J. Pan and J. Gong, *Coupled-wire construction of static and Floquet second-order topological insulators*, Phys. Rev. B **99**, 045441 (2019), doi:10.1103/PhysRevB.99.045441.
- [75] B. Huang and W. V. Liu, *Floquet higher-order topological insulators with anomalous dynamical polarization*, Phys. Rev. Lett. **124**, 216601 (2020), doi:10.1103/PhysRevLett.124.216601.
- [76] E. Khalaf, W. A. Benalcazar, T. L. Hughes and R. Queiroz, *Boundary-obstructed topological phases*, arXiv preprint arXiv:1908.00011 (2019).
- [77] H. Hu, B. Huang, E. Zhao and W. V. Liu, *Dynamical singularities of Floquet higher-order topological insulators*, Phys. Rev. Lett. **124**, 057001 (2020), doi:10.1103/PhysRevLett.124.057001.
- [78] J. K. Asbóth, B. Tarasinski and P. Delplace, *Chiral symmetry and bulk-boundary correspondence in periodically driven one-dimensional systems*, Phys. Rev. B **90**, 125143 (2014), doi:10.1103/PhysRevB.90.125143.
- [79] F. Merz and J. T. Chalker, *Two-dimensional random-bond Ising model, free fermions, and the network model*, Phys. Rev. B **65**, 054425 (2002), doi:10.1103/PhysRevB.65.054425.
- [80] B. Tarasinski, J. K. Asbóth and J. P. Dahlhaus, *Scattering theory of topological phases in discrete-time quantum walks*, Phys. Rev. A **89**, 042327 (2014), doi:10.1103/PhysRevA.89.042327.
- [81] M. Xiao, G. Ma, Z. Yang, P. Sheng, Z. Q. Zhang and C. T. Chan, *Geometric phase and band inversion in periodic acoustic systems*, Nature Physics **11**, 240–244 (2015), doi:10.1038/nphys3228.
- [82] M. Serra-Garcia, R. Süsstrunk and S. D. Huber, *Observation of quadrupole transitions and edge mode topology in an LC circuit network*, Phys. Rev. B **99**, 020304(R) (2019), doi:10.1103/PhysRevB.99.020304.
- [83] X. Zhu, *Tunable Majorana corner states in a two-dimensional second-order topological superconductor induced by magnetic fields*, Phys. Rev. B **97**, 205134 (2018), doi:10.1103/PhysRevB.97.205134.
- [84] Y. Volpez, D. Loss and J. Klinovaja, *Second-order topological superconductivity in π -junction rashba layers*, Phys. Rev. Lett. **122**, 126402 (2019), doi:10.1103/PhysRevLett.122.126402.
- [85] T. E. Pahomi, M. Sigrist and A. A. Soluyanov, *Braiding Majorana corner modes in a two-layer second-order topological insulator*, arXiv preprint arXiv:1904.07822 (2019).
- [86] S. Franca, D. V. Efremov and I. C. Fulga, *Phase-tunable second-order topological superconductor*, Phys. Rev. B **100**, 075415 (2019), doi:10.1103/PhysRevB.100.075415.

- [87] A. Altland and M. R. Zirnbauer, *Nonstandard symmetry classes in mesoscopic normal-superconducting hybrid structures*, Phys. Rev. B **55**, 1142 (1997), doi:10.1103/PhysRevB.55.1142.
- [88] L. Fu, C. L. Kane and E. J. Mele, *Topological insulators in three dimensions*, Phys. Rev. Lett. **98**, 106803 (2007), doi:10.1103/PhysRevLett.98.106803.
- [89] Z. Ringel, Y. E. Kraus and A. Stern, *Strong side of weak topological insulators*, Phys. Rev. B **86**, 045102 (2012), doi:10.1103/PhysRevB.86.045102.
- [90] A. Milsted, L. Seabra, I. C. Fulga, C. W. J. Beenakker and E. Cobanera, *Statistical translation invariance protects a topological insulator from interactions*, Phys. Rev. B **92**, 085139 (2015), doi:10.1103/PhysRevB.92.085139.